Complex brecciation and shock effects in the Buck Mountain Wash (H3–5) chondrite

Melinda HUTSON[1*], Alex RUZICKA[1], Richard PUGH[1], Larry SLOAN[2], and Edwin THOMPSON[3]

[1]Cascadia Meteorite Laboratory, Department of Geology, Portland State University,
17 Cramer Hall, 1721 Southwest Broadway, Portland, Oregon 97207–0751, USA
[2]13507 CR 2½, Brighton, Colorado 80603, USA
[3]ET Meteorites, 16869 Southwest 65th Avenue #331, Lake Oswego, Oregon 97035, USA
[*]Corresponding author. E-mail: mhutson@pdx.edu

Abstract–Buck Mountain Wash (BMW) is a new genomict breccia (H3–5) found in the Franconia (H5) strewn field in Arizona that shows complex brecciation and shock effects. It contains three distinct chondritic lithologies in sharp contact: a) a main lithology that consists primarily of petrographic type 5 material but which has finely intermixed type 3 and 4 material, b) a shock-blackened (shock stage S5) type 3 lithology (lithology A), and c) a shock-blackened type 3/4 lithology (lithology B). Buck Mountain Wash was lithified after impact-mixing and impact-melting of weakly and strongly metamorphosed materials, possibly at depth in the regolith of the parent body. Shock effects included brecciation on a fine scale, localized impact-melting of silicates, partial melting, and mobilization of metal-sulfide, and chemical fractionations that produced non-H-group composition kamacite by two disequilibrium mechanisms. Shock heating did not cause significant thermal metamorphism in the shock-blackened lithologies of BMW, except possibly in areas adjacent to whole-rock shock melt. During lithification, cooling must have been rapid at high temperatures to preserve glass and inhomogeneous silicate compositions, but not so fast at lower temperatures as to produce dendritic metal-sulfide globules or martensite.

INTRODUCTION

Since the discovery of the Franconia (H5) chondrite in 2002 (Russell et al. 2004), well over 100 individual meteorite specimens (chondrites and irons) have been recovered from a small (~10 km radius) area in Mohave County, Arizona, USA, known as the Franconia strewn field (Bleacher et al. 2005). An 816 g stony meteorite was found in this area on January 28, 2004, by Larry Sloan, who sent pieces of this stone to the Cascadia Meteorite Laboratory (CML) for classification. Upon examination it quickly became apparent that this stone, Buck Mountain Wash (BMW), was not paired with the Franconia meteorite. Additionally, the classification of BMW was complicated because it contained chondritic clasts that experienced diverse thermal and shock histories, as well as small-scale brecciation within the clasts. In this report, we present a detailed description of an interesting impact breccia that shows complex mechanical and chemical phenomena.

SAMPLES AND ANALYTICAL TECHNIQUES

CML received a 21 g end piece of BMW from which four doubly polished thin sections were prepared (0144-3, 0144-4, 0144-7A, and 0144-7B). Two additional slices (totaling 59 g) from the same specimen were also donated to CML. Preliminary information on classification (Russell et al. 2005) lists a mass for the total specimen of 798 g and for the type specimen of 34.7 g. Both of these masses are incorrect for different reasons. The mass of the type specimen is incorrect because additional material was provided by the finder following submission of the classification, whereas the reported total mass is too low due to a miscommunication. Correct values are 816 g for the total specimen and 80 g for the type specimen.

The thin sections were studied using optical microscopy, scanning electron microscopy (SEM), and electron microprobe (EMP) analysis. SEM work was performed at Portland State University using a JEOL JSM-35C with a Kevex energy dispersive detector and 4pi digital image/spectrum acquisition system. Backscattered electron (BSE) images and X-ray maps were obtained with the SEM. BSE observations were performed using two settings: one suitable for silicates, and the other for metal. EMP analyses of olivine, pyroxene, plagioclase, glass, and metal were obtained at Oregon State University with Cameca SX-50 and SX-100 electron microprobes using wavelength dispersive
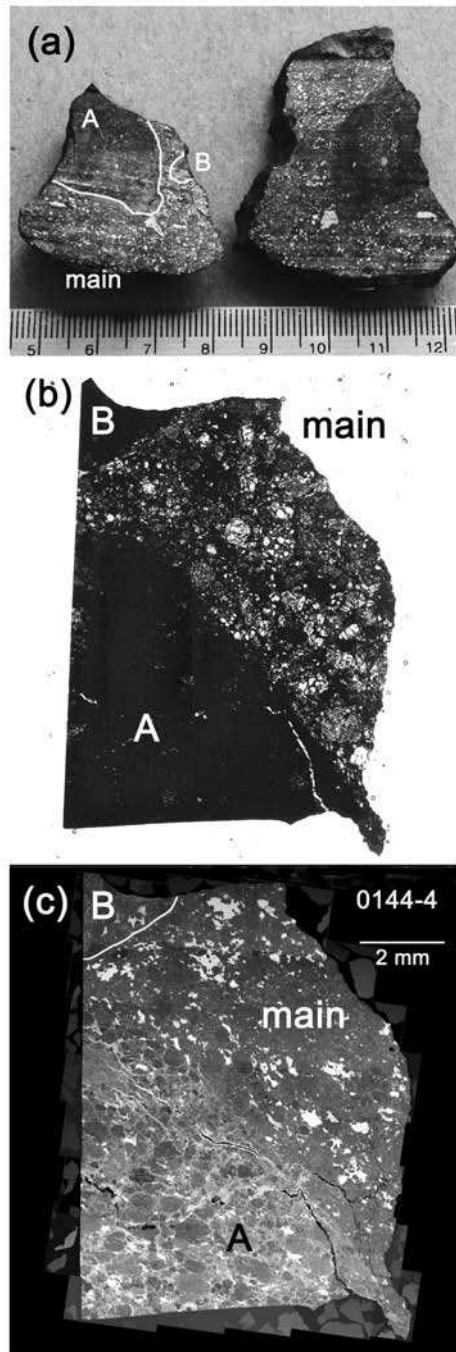
Fig. 1. a) View of cut surfaces of BMW showing opposing faces in hand specimen. Lithologies A and B are dark clasts and are depleted in coarse metal. Lithology A has a metal-depleted border in contact with the main lithology (right piece). The scale bar is in centimeters with millimeter subdivisions. A thin slice was cut perpendicularly through the cut face in the left specimen across all lithologies; this slice was used to create polished thin section (PTS) 0144-4. b) Transmitted light image of PTS 0144-4, showing the opaque nature of lithologies A and B and chondrules in the main lithology. c) BSE image of 0144-4, showing coarser metal grains (bright) in the main lithology, some of which are aligned parallel to the contacts of lithologies A and B, and well-defined unequilibrated chondrules in lithology A (darker and lighter shades of medium gray).

spectrometers. All phases except for plagioclase and glass were analyzed with an accelerating voltage of 15 kV, a 50 nA sample current, and a beam focused to a diameter of ~1 μm; for plagioclase and glass, a 10 nA sample current and a beam ~4 μm in diameter were used instead. Detection limits (95% confidence) for elements calculated using Cameca-supplied software indicates typical values of 0.01–0.04 wt% for silicates, except for Fe and Ni (0.07–0.08 wt%), and values of 0.01 wt% for P, 0.03–0.04 wt% for Cr, and 0.11–0.13 wt% for Fe, Ni, and Co in metal.

RESULTS

Petrography

Overview

Figure 1 shows macroscale features of BMW in hand specimen (Fig. 1a), in thin section in transmitted light (Fig. 1b), and in a BSE image mosaic (Fig. 1c). Three lithologies with reasonably sharp contacts with one another can be defined. The main lithology comprises the bulk of BMW and has a chondritic texture (Fig. 1b) with abundant metal grains (Figs. 1a and 1c). A few notably larger metal grains are visible in hand specimen (Fig. 1a). Lithology A is dark in hand specimen (Fig. 1a). In some sections, lithology A is opaque in transmitted light (Fig. 1b), whereas in other sections it is more transparent. It consists of a completely opaque, metal-depleted border zone (~0.5 cm thick) surrounding a central region where chondrules and fine-grained metal are visible (Fig. 1a, right). The metal in lithology A is notably finer-grained than in the main lithology (Figs. 1a and 1c). In BSE images (Fig. 1c), the chondrules in lithology A appear well-defined and highly variable in composition (dark and light shades of gray). Lithology B is dark in hand specimen and opaque in transmitted light (Fig. 1b). Part of lithology B contains metal grains of a similar size to that in the main lithology, while another part of lithology B is devoid of coarse metal (Fig. 1c). Roughly 10% of the metal in the main lithology has been replaced by iron oxides during terrestrial weathering, consistent with a weathering grade of W1 (Wlotzka 1993). Lithologies A and B are more fractured which appears to have resulted in a slightly higher degree of weathering, with up to 20% replacement of opaques.

Main Lithology

In thin section, the margins of chondrules in the main lithology appear somewhat indistinct, reminiscent of a type 5 ordinary chondrite. Most olivine grains in this lithology show weak undulose extinction with irregular or a few planar fractures, although some grains show stronger undulose extinction and have multiple planar fractures. Using the shock classification of Stöffler et al. (1991), this suggests that the main lithology was shocked predominantly to shock stage S2, with some regions shocked to stage S3.

In BSE images, it is apparent that the majority of olivine and pyroxene grains in this lithology are chemically uniform and that some coarser aggregates of feldspar (up to ~70 μm across) are present (Fig. 2a). These aggregates appear to be composed of grains that are roughly 10–25 μm across, consistent with a petrographic grade of type 5 (Sears and Dodd 1988; Hutchison 2004). Most chondrules are fragments of larger objects and display a wide range of sizes. Figure 2b shows a relatively large (~350 μm long) oblate fragment of a porphyritic olivine chondrule with a partial rim of pyroxene. A slightly smaller fragment (~200 μm long) of an object with parallel olivine bars and intervening feldspar may be a fragment of a much larger barred olivine chondrule (Fig. 2c). Smaller fragments of chondrules (≤50 μm across) are visible in Fig. 2d, including an elongated fragment of a porphyritic olivine-pyroxene (POP) chondrule. These small chondrule fragments appear to comprise all or much of the matrix of the main lithology (Fig. 2d). In the thin section containing all three lithologies, the long axes of elongate chondrule fragments in the main lithology (Figs. 2b–d) tend to be oriented roughly parallel to the contact with lithology A (upper left to lower right in Fig. 2). This is not the case for silicate in a thin section made of the main lithology farther from lithology A, suggesting it is a local alignment present close to the contact of lithology A.

Although most of the ferromagnesian silicates appear to be compositionally uniform in BSE, a few objects containing other compositions of olivine and pyroxene are present. In Fig. 2c, the object at lower right is a largely circular porphyritic olivine chondrule that contains Mg-rich olivine set in glass, which is clearly in chemical disequilibrium and texturally out of place with its surroundings. This chondrule is characteristic of type 3 metamorphic grade. There is no evidence for chemical exchange between this Mg-rich chondrule and its more ferrous surroundings. More evidence for chemical disequilibrium is provided by the oblate chondrule fragment with a partial pyroxene rim (Fig. 2b), which contains chemically uniform olivine similar to that present elsewhere in the main lithology, but zoned pyroxene in the rim which is atypically magnesian. This chondrule also contains a devitrified feldspathic groundmass. These characteristics are consistent with a type 4 metamorphic grade for this chondrule.

Most of the metal grains in the main lithology consist of featureless kamacite or taenite grains, or featureless kamacite grains with tetrataenite borders (Fig. 3a). No plessite or evidence of martensite was found. Rarely, kamacite grains contain stringers or blebs of Ni-rich metal (Fig. 3b). These stringers, which are <3 μm wide and up to 50 μm long, are oriented within the grains, suggesting that they formed by exsolution. Some metal grains contain globular inclusions of Ca phosphate.

Larger aggregates of metal partially to completely surround and embay silicate grains and chondrules (Figs. 2a and 2e). Metal fills interstices between silicates, both at the edges of chondrules (e.g., Fig. 2e, left and right) and between grains that could have been derived from chondrules (e.g., Fig. 2e, upper right). In the thin section containing lithologies A and B, metal grains are weakly foliated in the main lithology (upper left to lower right of Figs. 1c and 2a), primarily parallel to the contact with lithology A, and possibly also parallel to the contact with lithology B (Fig. 1c). The metal foliation parallels the direction in which elongated chondrule fragments are oriented (Figs. 2b–d).

Lithology A

Lithology A has characteristics typical of type 3 material. These include ferrous and magnesian chondrules adjacent to one another (Fig. 4a), abundant glass inside chondrules (Figs. 4b and 4c), zoned olivine and pyroxene grains, dusty-olivine-bearing chondrules (Fig. 4c), and fine-grained FeO-rich matrix (Fig. 4b). Most chondrules are oblate (Fig. 4a) and fragmented on a small scale (Fig. 4b). Long axes of chondrules are roughly parallel to one another, producing an overall foliation, which is not parallel to the contact with the main lithology (Fig. 1c). Matrix appears to be much less abundant than in a typical type 3 chondrite (10–15 vol%) (Brearley and Jones 1998), consisting of isolated patches found between tightly fitting chondrules (Figs. 4a and 4b). Using BSE images, the maximum and minimum diameters of 105 chondrules were measured and averaged. The average size of chondrules was 0.36 mm, with a standard deviation of 0.16 mm. This is consistent with lithology A being an H-group chondrite (Brearley and Jones 1998; Scott and Krot 2005).

Most areas of lithology A are opaque in transmitted light because of the presence of small inclusions and veins of metal and troilite inside silicates. Additionally, silicates are cut by glassy silicate and troilite veins that contain small drop-formed masses of metal. These effects are typical of shock-blackened chondrites (e.g., Dodd 1981; Rubin 1992).

In some areas, lithology A was sufficiently transparent in transmitted light that internal deformation features of silicates could be studied. A preponderance of olivine grains show strong mosaic extinction and multiple sets of planar fractures, although examples of olivine grains with undulose or slightly mosaic extinction are present. These characteristics imply that lithology A experienced shock pressures consistent with shock stage S5 (Stöffler et al. 1991), with some regions more typical of shock stages S3 to S4.

In contrast to those in the main lithology, the sulfides in lithology A do not form large discrete grains. Instead, troilite is found exclusively as small (<50 μm across) grains, droplets, and veins, some of them containing metal inclusions (Fig. 3e). Owing to this small size, the total abundance of troilite in lithology A is difficult to estimate, but it appears to be subchondritic. Additionally, troilite often forms a lacy network that contains silicate grains (Fig. 3f).
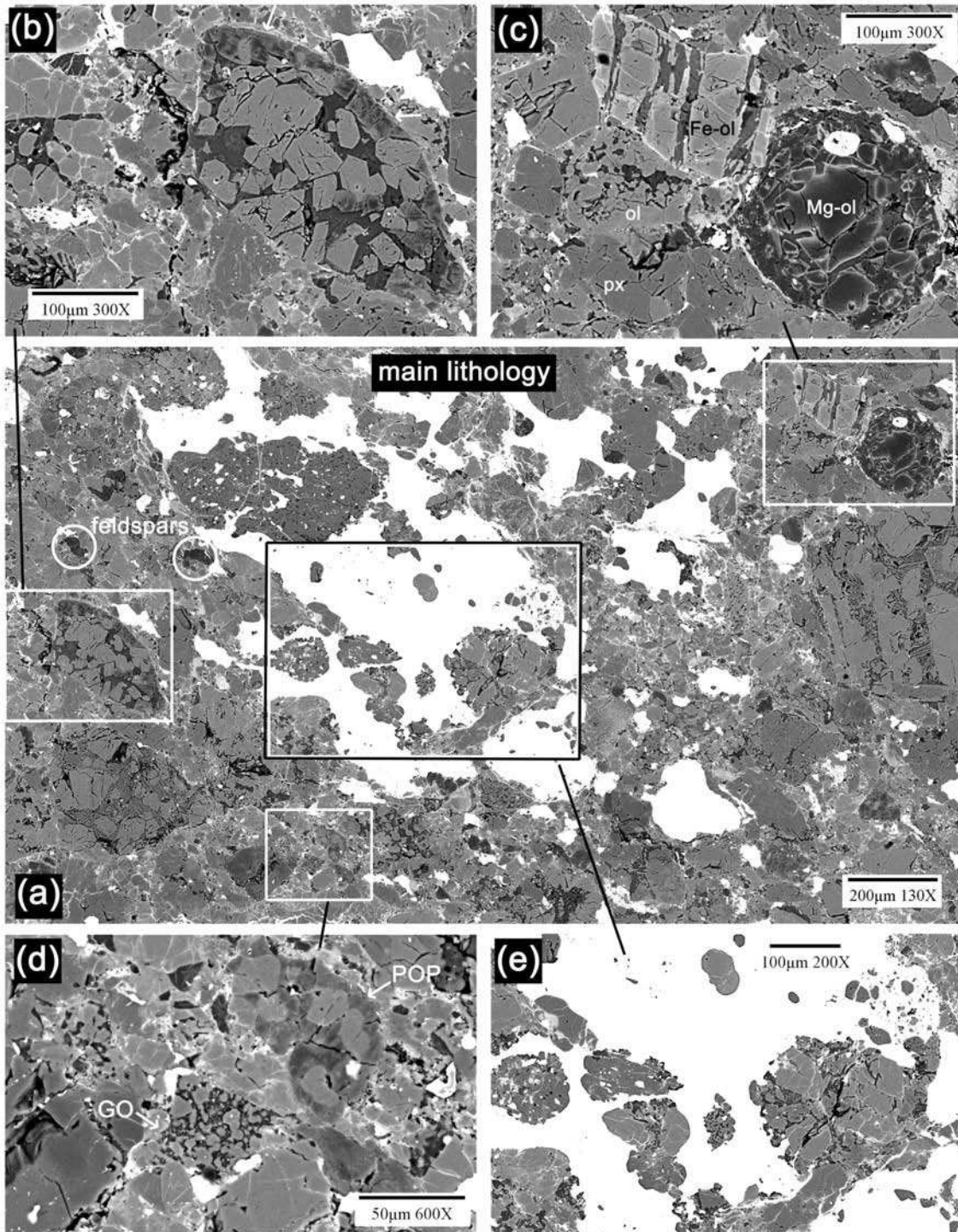
Fig. 2. BSE images of the main lithology showing an overview and higher-magnification images. a) Equilibrated silicates (same shade of gray) are dominant in this overview of the main lithology, which also contains some coarser feldspars ($Ab_{80-81}Or_5$). b) Oblate chondrule fragment containing equilibrated olivine (Fo_{81}) and a partial rim of zoned low-Ca pyroxene (arrows) set in a devitrified feldspathic glass, typical of type 4 chondritic material. c) The magnesian chondrule at the lower right contains zoned olivine (Mg-ol, Fo_{92-97}) set in glass and is in direct contact with a chondrule fragment containing Fe-rich olivine (Fe-ol, Fo_{80}) bars separated by feldspathic material ($Ab_{22}Or_{0.3}$). The surroundings are dominated by equilibrated olivine (ol, Fo_{80-81}) and slightly zoned low-Ca pyroxene (px, En_{78-83}). d) Example of small-scale brecciation in the main lithology, showing small (50–100 µm in diameter) chondrule fragments, including objects with granular olivine (GO) and porphyritic olivine-pyroxene (POP) textures. e) Apparently fluidized metal encloses individual chondrules (left and center) as well as grains that could have been disaggregated from chondrules (upper right).
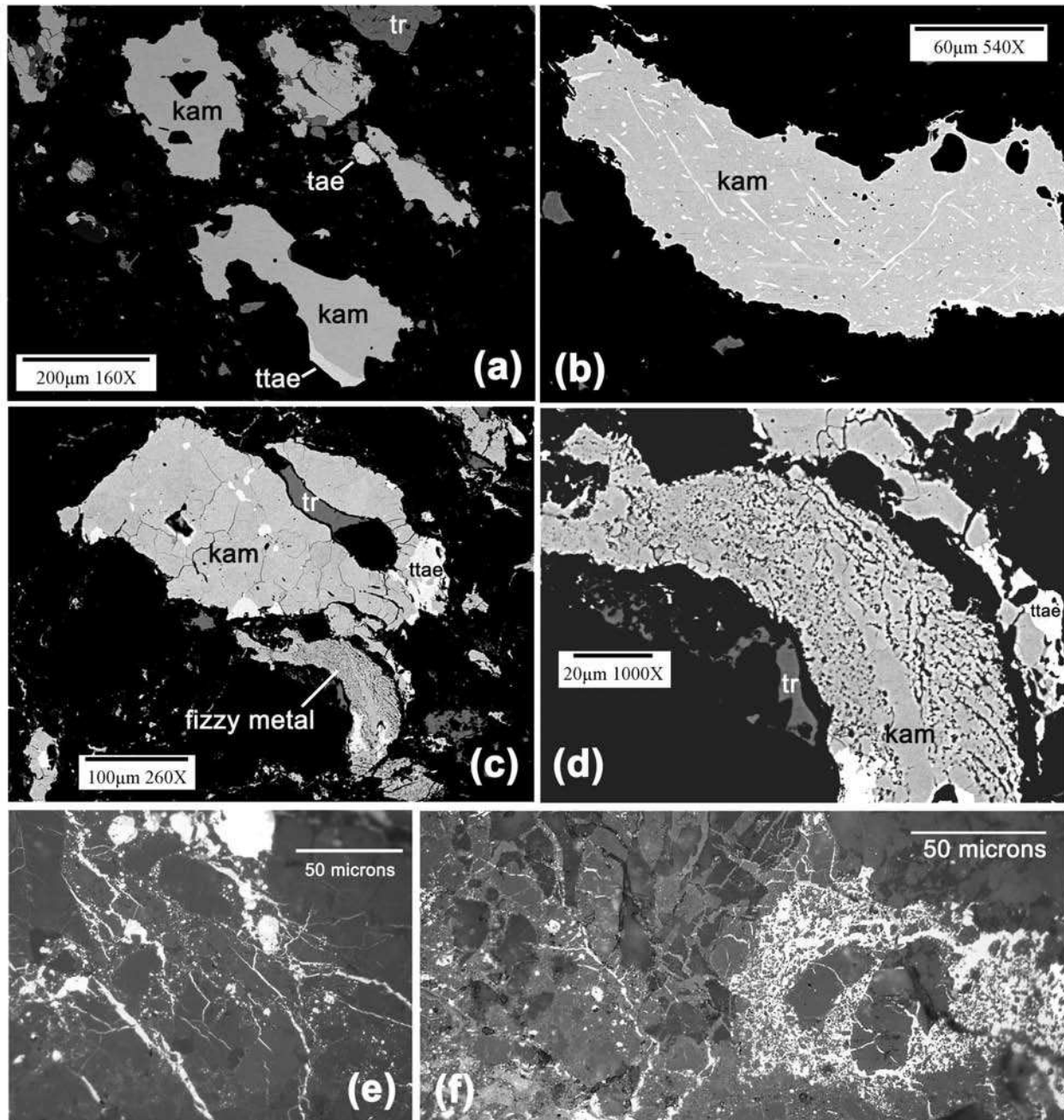
Fig. 3. BSE (a–d) and reflected light (e–f) images of metal-troilite textures. a) Typical normal metal in the main lithology showing kamacite (kam), taenite (tae), and tetrataenite (ttae). Grains have homogenous interiors. tr = troilite. b) Rare kamacite with anomalous composition in the main lithology, containing Ni-rich needles and blebs (white). c) Polycrystalline kamacite intergrown with tetrataenite and "fizzy metal" in lithology A. d) Closer view of fizzy metal from part (c), showing metal filled with tiny silicate and troilite inclusions (dark). e) Veins and droplets of metal and troilite (bright) associated with silicate melt pockets in lithology A. Veins are largely troilite, but contain metal globules. f) Lacy troilite (bright, right) appears to have flowed around silicates. Troilite veins and globules appear at left.

No plessite was observed in lithology A. Coarse metal in this lithology consists of two broad textural types, which somewhat grade into one another. One endmember consists of adjoining kamacite grains and Ni-rich metal (taenite and tetrataenite) between kamacite grains (Fig. 3c). Many of the grains meet at approximately 120° intersections, consistent with the polycrystalline kamacite described by Bennett and McSween (1996). Polycrystalline metal is believed to be related to shock reheating, characteristic of a shock stage of S5 or S6 (Bennett and McSween 1996). The other endmember, which tends to be smaller than the polycrystalline metal, consists of aggregates of kamacite
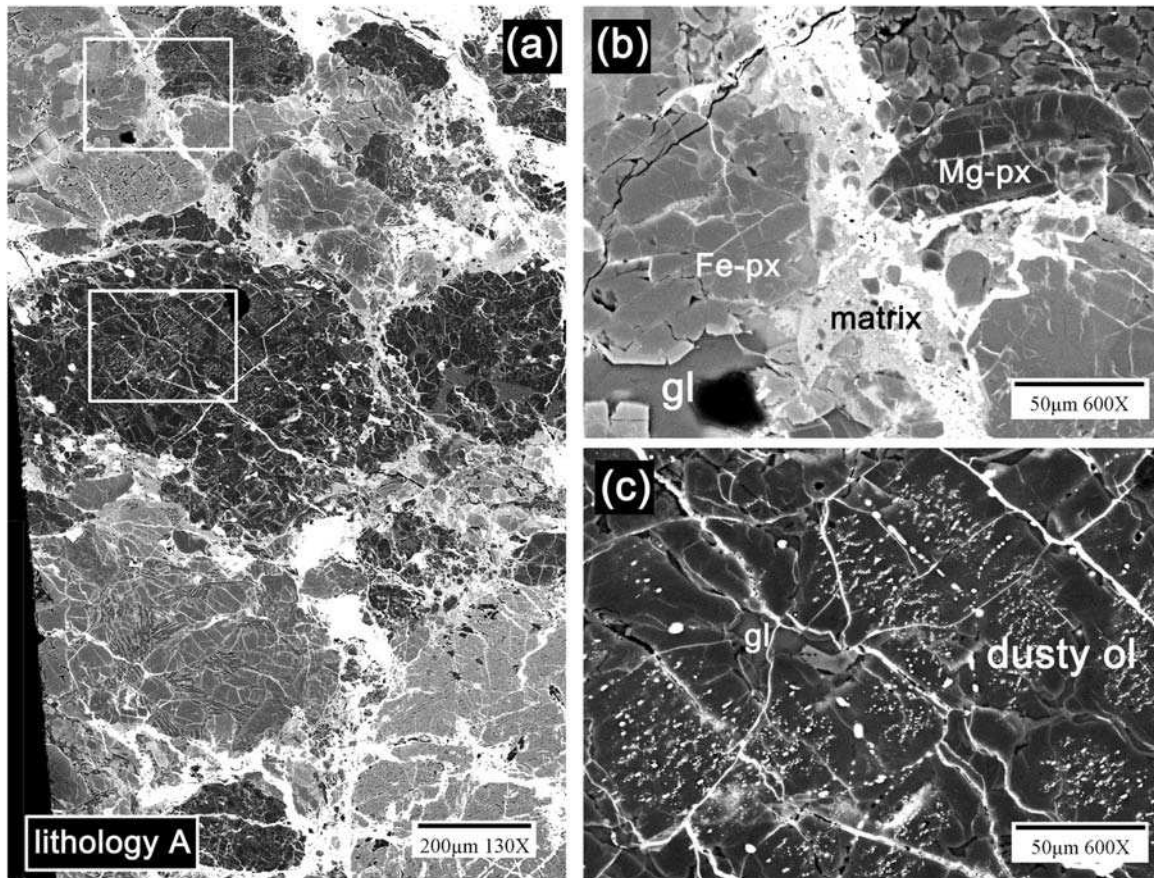
Fig. 4. BSE images of lithology A. a) Overview showing chondrules dominated by a mixture of magnesium-rich silicates (dark) or iron-rich silicates (light gray), typical of a type 3 chondrite. Chondrules are tightly packed and foliated (long axes in left-right direction). The boxed regions are shown in greater detail in parts (b) and (c). b) Higher magnification view showing a small amount of Fe-rich matrix (bright) between three chondrules with broken margins, which contain glass (gl) and pyroxene (px) of varied compositions. c) Higher magnification view showing chondrule containing glass (gl) and magnesian olivine (dark) with dusty metal (bright inclusions).

intergrown with tiny (<1–2 μm wide) inclusions of silicate and occasional troilite (Fig. 3d). The proportion of metal to silicate varies widely from one object to another. We refer to these metal-rich aggregates as "fizzy metal," analogous to the "fizzy troilite" described by Bennett and McSween (1996), but consisting primarily of metal and not troilite. The two types of metal—polycrystalline and fizzy—can occur adjacent to one another (Fig. 3c) or as separate objects. Elongate coarse metal particles in lithology A are roughly aligned with the silicate foliation.

Lithology B

No silicates in lithology B could be observed in transmitted light, precluding a determination of a shock stage for this lithology. However, it is clear that lithology B has been extensively shocked. This lithology appears dark in hand specimen and opaque in transmitted light because of the presence of numerous tiny opaque inclusions, typical of shock blackening.

Lithology B has two texturally distinct portions when examined with BSE. Most of lithology B visible in Fig. 5b contains relatively sparse, large metal grains similar to those in the main lithology. Although the exposed section of lithology B is small, it does not show some of the characteristic features of the main lithology, including chondrule fragments, or highly magnesian silicates (dark in BSE).

Along the edge of the section, lithology B consists of a shock melt with slightly zoned olivine and pyroxene grains enclosed in feldspathic glass (Figs. 5a and 5b). The grains are zoned normally with narrow ferrous rims on magnesian cores. This shock melt contains numerous drop-formed and irregularly shaped opaque grains (~5 μm in diameter), most of which are metal, although some are troilite. A portion of this melt zone consists of what appears to be a brecciated relict chondrule that contains primarily olivine grains invaded by veins of troilite (Fig. 5a). The troilite veins are truncated at the edge of this object, suggesting that the shock melt solidified after incorporation of the relict chondrule.
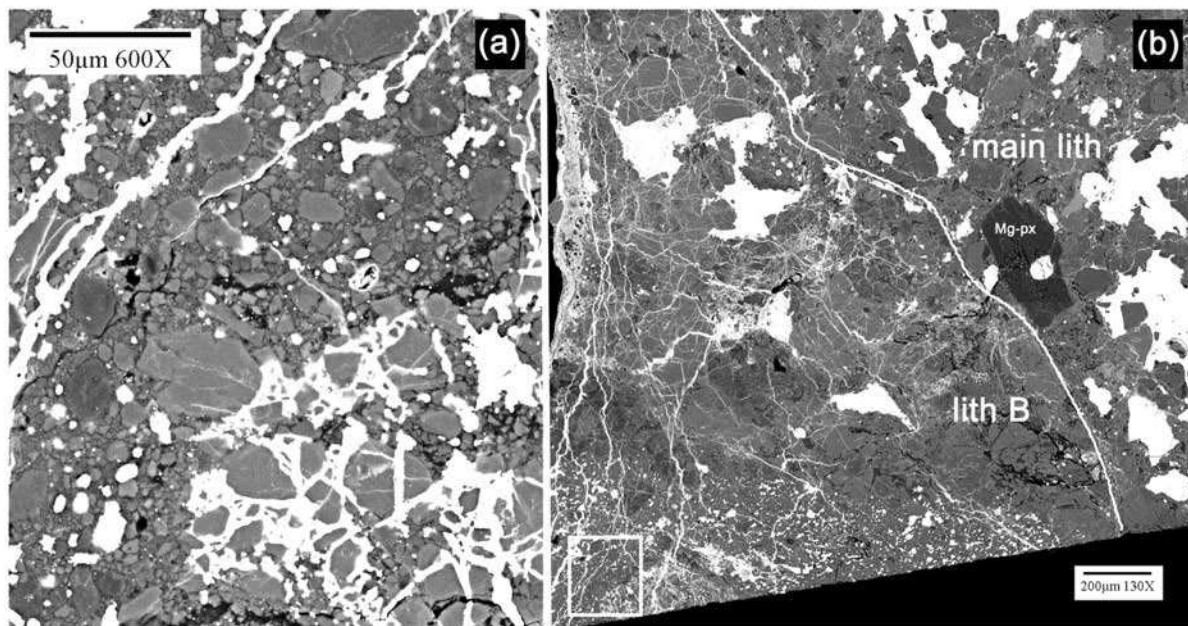
Fig. 5. BSE images of lithology B. a) Shock-melted portion, including relict olivine-rich chondrule with prominent troilite veins (bright, lower right) and surrounding melt zone containing euhedral grains of olivine, low-Ca pyroxene, drop-formed metal of variable P content (bright), and rare troilite. The bright veins at upper left are composed of weathering products. b) Overview of lithology B, showing location of part (a), and the contact between lithology B and the main lithology. The shock-melt zone occurs along the bottom edge of the section; fusion crust occurs at the extreme left edge. Most of lithology B contains larger, irregularly shaped metal grains that do not contain elevated P.

Phase Compositions

Silicates

A large number (290) of EMP analyses were obtained of silicates in Buck Mountain Wash so as to determine representative compositions of each lithology. In addition, BSE images were used to target analyses of grains with extreme compositions. Figures 6 and 7 show histograms of fayalite in olivine and ferrosilite in low-Ca pyroxene for the three lithologies. The average compositions (and standard deviations) of olivine and low-Ca pyroxene in all three lithologies and feldspar in the main lithology are given in Table 1.

Olivine and low-Ca pyroxene in the main lithology are predominantly equilibrated, with over half the analyses having compositions (Fa_{18-20}; Fs_{16-18}) typical of an equilibrated H-group chondrite (Figs. 6a and 7a). However, the total range of compositions is much larger ($Fa_{0.5-35.6}$; $Fs_{1.6-31.5}$) (Figs. 6a and 7a), indicating an admixture of unequilibrated material. In addition, of the 55 analyzed olivines having fayalite contents in the equilibrated H-group range (Fa_{16-20}), 44 (80%) have CaO contents ≤0.05 wt%, suggesting that the majority of this lithology consists of material of petrographic type 5 or 6 (Dodd 1981, p. 85). Of the 39 pyroxene analyses in the equilibrated H-group range ($Fs_{14.5-18}$), roughly 90% have Wo contents (0.5–2.0 mol%) consistent with equilibrated (type 4–6) H-group chondrites (Brearley and Jones 1998; Dodd 1981). Relatively coarse

feldspars in this lithology are fairly uniform in composition ($Ab_{78.8-80.5}$ $An_{14.4-18.4}$ $Or_{2.8-5.1}$) (Table 1).

Both olivine Fa and low-Ca pyroxene Fs contents vary widely in lithology A (Figs. 6b and 7b). The fayalite distribution in olivine peaks broadly around the H-group equilibrated range (Fig. 6b). Twenty of 40 olivine analyses in lithology A have Fa contents either within the range for H4–6 chondrites or lie within 2 mol% above or below this range. Scott (1984) showed that various type 3.6–3.7 H and L chondrites had Fa distributions stongly peaked in the corresponding equilibrated range, suggesting that group assignments can be made for mildly metamorphosed type 3 chondrites based on olivine compositions. However, CaO contents in all but one olivine analysis are ≥0.10 wt%, suggesting that this lithology contains little, if any, equilibrated (types 4–6) H-group material (Dodd 1981). The coefficient of variation for fayalite in olivine in lithology A is 50.5, which implies a high type 3.4 (Sears and Dodd 1988; Hutchison 2004). Similarly, all but two of the analyzed pyroxenes fall outside the equilibrated H-group range in terms of Fs (Fig. 6b) and Wo, which is consistent with type 3 material.

The data for olivine and pyroxene compositions in lithology B are not readily pigeonholed into a particular petrographic type. The iron contents of olivine and low-Ca pyroxene in this lithology are not as variable as in lithology A (Table 1), but extend outside of the range for equilibrated (types 4–6) chondrites (Figs. 6c and 7c). Most olivine
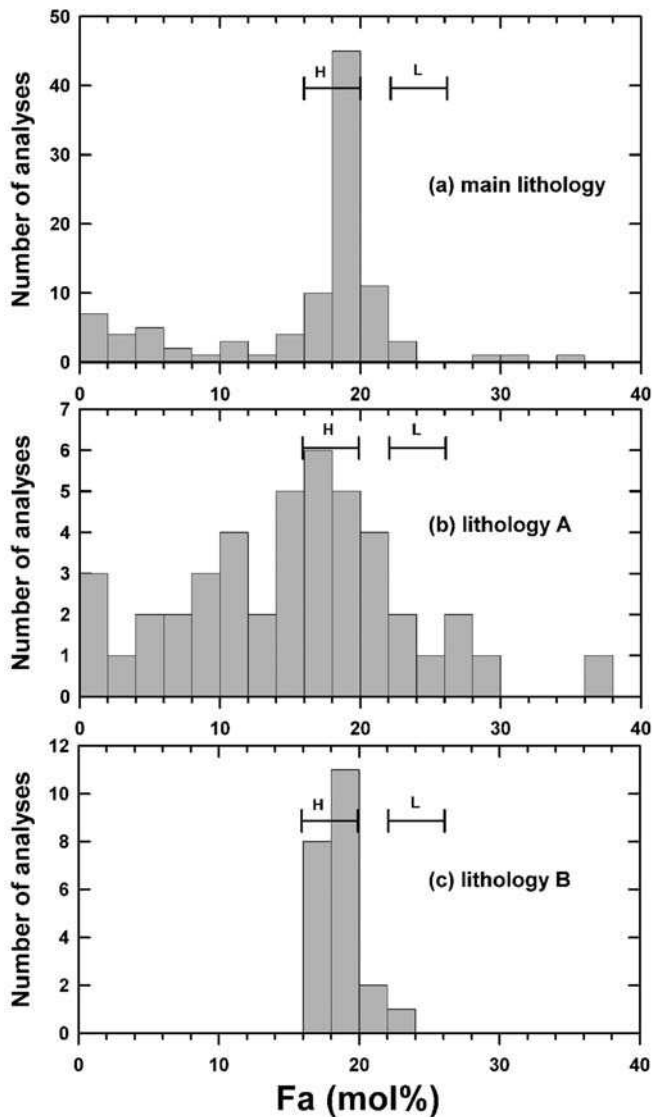
Fig. 6. Histograms of olivine Fa content in (a) the main lithology, (b) lithology A, and (c) lithology B. Ranges for equilibrated (types 4–6) H and L chondrites (Dodd 1981) are shown. For the main lithology, an attempt was made to sample grains of different compositions, so the relative proportion of equilibrated olivine is somewhat underestimated.
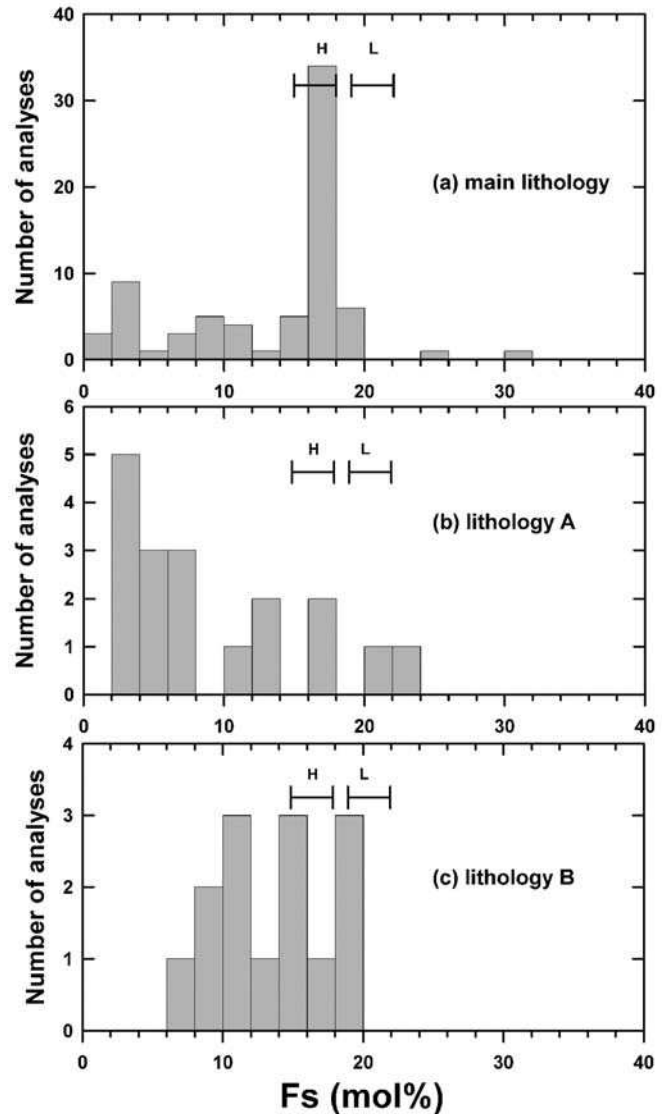

Fig. 7. Histograms of low-Ca pyroxene Fs content in the three lithologies of BMW. Ranges for equilibrated (types 4–6) chondrites are from Dodd (1981).

compositions fall within the H4–6 range (Fig. 6c). The most ferrous olivine compositions in this lithology correspond to the rims of zoned grains in the shock-melted portion; excluding these grains, the coefficient of variation of Fa in olivine is 2.1, which is consistent with an equilibrated chondrite. All but four olivine analyses in the H-group range (Fa$_{16-20}$) have CaO contents of <0.1 wt%, which is consistent with a type 4–6 designation (Dodd 1981), but the CaO contents in the remaining grains are up to ~0.45 wt%. Ferrosilite contents (Fig. 7c) and Wo contents in pyroxene suggest that both the shock-melted and unmelted portions of lithology B are unequilibrated.

Metal

Kamacite compositions vary systematically between the three lithologies in Buck Mountain Wash. Table 2 shows selected EMP data for kamacite that illustrate normal and more extreme compositions. Cobalt, P, and Ni contents in kamacite in the three lithologies of BMW are compared to that in H3–6 and L3–6 chondrites in Figs. 8a and 8b.

Nickel and Co contents in kamacite in the main lithology cluster around H-group values (Fig. 8a; note 1 in Table 2), except for four analyses that have anomalously low Ni contents (≤4 wt%). These analyses are of four grains that are the only ones observed in the main lithology containing small fibers and blebs of high-Ni metal (Fig. 3b). Two of these anomalous grains also have unusually high Co contents (>0.55 wt%, see note 2 in Table 2).

Table 1. Average composition of silicates in Buck Mountain Wash, determined by electron microprobe analysis. Values in parentheses are the standard deviation of the mean; N = number of analyses, n.a. = not analyzed.

Phase	Olivine			Pyroxene			Feldspar
Lithology	Main	A	B[a]	Main	A	B[b]	Main
wt%							
SiO_2	39.5 (1.3)	39.5 (1.4)	39.2 (0.5)	56.5 (1.3)	56.9 (1.9)	56.3 (1.1)	65.3 (1.0)
TiO_2	0.02 (0.03)	0.01 (0.02)	0.02 (0.03)	0.10 (0.08)	0.03 (0.05)	0.02 (0.02)	0.04 (0.04)
Al_2O_3	0.06 (0.07)	0.06 (0.06)	0.11 (0.21)	0.38 (0.48)	0.47 (0.61)	0.26 (0.15)	22.2 (0.4)
Cr_2O_3	0.09 (0.28)	0.21 (0.10)	0.10 (0.26)	0.29 (0.25)	0.69 (0.25)	0.36 (0.16)	0.04 (0.07)
FeO	15.1 (6.3)	14.5 (6.9)	17.5 (1.0)	9.07 (4.12)	6.22 (4.11)	9.54 (2.45)	0.54 (0.12)
MnO	0.35 (0.16)	0.31 (0.14)	0.44 (0.05)	0.38 (0.14)	0.33 (0.23)	0.29 (0.15)	0.01 (0.02)
MgO	44.9 (5.1)	45.4 (5.6)	43.1 (1.4)	32.5 (3.0)	34.7 (3.6)	32.8 (2.4)	0.06 (0.11)
NiO	0.03 (0.05)	0.08 (0.06)	0.06 (0.06)	0.02 (0.03)	0.06 (0.03)	0.08 (0.11)	n.a.
CaO	0.14 (0.17)	0.17 (0.09)	0.08 (0.12)	0.67 (0.48)	0.46 (0.59)	0.45 (0.40)	3.00 (0.40)
Na_2O	<0.01 (0.01)	0.01 (0.02)	0.01 (0.02)	0.01 (0.02)	0.02 (0.03)	0.02 (0.02)	8.96 (0.27)
K_2O	n.a.	n.a.	n.a.	n.a.	n.a.	n.a.	0.97 (0.20)
Total	100.15	100.31	100.57	100.51	100.00	100.17	101.17
mol%							
Fa	16.1 (6.9)	15.4 (7.8)	18.6 (1.4)				
Wo				1.3 (0.9)	0.9 (1.2)	0.9 (0.8)	
En				85.3 (6.4)	89.9 (6.9)	85.2 (4.1)	
Fs				13.5 (6.2)	9.2 (6.3)	14.0 (3.8)	
Ab							79.6 (1.5)
An							14.7 (2.1)
Or							5.7 (1.1)
N	99	44	22	73	18	14	16

[a]Consists of 17 analyses from unmelted portion, and 5 analyses from melted portion. Latter olivine ranges from $Fa_{18.9-22.7}$.
[b]Consists of 12 analyses from unmelted portion, and 2 analyses from melted portion. Latter pyroxene ranges from $Fs_{11.9-18.1}$.

Table 2. Selected compositions (wt%) of kamacite in Buck Mountain Wash, determined by electron microprobe analysis. n.a. = not analyzed.

Lithology	Fe	Co	P	Cr	Ni	Total	Co/Ni wt.	Note[a]
Main	92.7	0.44	<0.01	0.02	6.56	99.76	0.067	1
Main	95.1	0.62	<0.01	0.10	3.98	99.81	0.156	2
A	93.5	0.55	<0.01	n.a.	5.04	99.08	0.108	3
A	94.6	0.85	0.01	0.02	4.33	99.79	0.196	4
B	92.9	0.34	<0.01	n.a.	6.49	99.76	0.052	5
B	90.3	0.28	0.37	n.a.	8.53	99.55	0.033	6

[a]1 = kamacite in main lithology similar to typical H chondrite; 2 = Ni-poor/Co-rich metal in main lithology; 3 = kamacite in lithology A most like main lithology; 4 = kamacite in lithology A least like main lithology; 5 = P-poor metal in lithology B outside of shock melt; 6 = P-rich metal in lithology B inside shock melt.
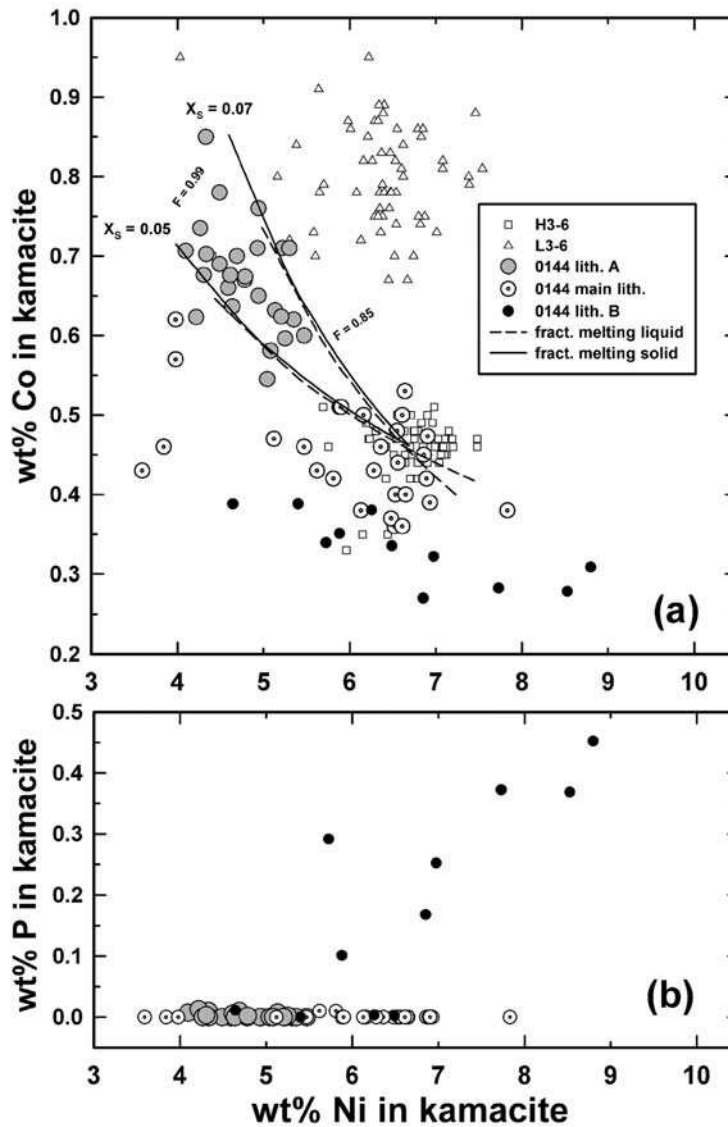
Fig. 8. Metal compositions in various lithologies of BMW compared to other H3–6 and L3–6 chondrites and to melting models. Metal compositions for typical H and L chondrites represent average compositions for individual meteorites (Afiattalab and Wasson 1980; Kong and Ebihara 1996; Kong et al. 1995; Rambaldi 1976, 1977; Rubin 1990; Smith et al. 1993), whereas BMW data represent individual analyses. a) Kamacite Co and Ni compositions. Lines show trends for liquid and solid metal during fractional melting of metal with typical H-group composition; X_S = atom fraction of S in metallic melt; F = fraction of melt corresponding to solid metal composition. Lithology A kamacite resembles the composition predicted for residual solid with 85–99% fractional melting and X_S = 0.05–0.07. b) Kamacite P and Ni compositions.

All the kamacite analyses in lithology A are of relatively large polycrystalline grains. In contrast to that in the main lithology, kamacite in lithology A is chemically distinct from that found in both H3–6 and L3–6 chondrites (Fig. 8a). This kamacite is characterized by simultaneously low Ni (4–5.5 wt%) and high Co (0.55–0.85 wt%) contents. Table 2 shows two extreme compositions for kamacite in lithology A, with a composition most similar to that in H chondrites (note 3) and least similar to that in H chondrites (note 4). The coefficient of variation for Co in kamacite in lithology A is 9.8, which implies a type 3.5 (Sears and Dodd 1988;

Hutchison 2004). This substantiates the high type 3.4 designation based on olivine iron content.

Kamacite in lithology B has Co and Ni contents overlapping that in H3–6 chondrites, but extending to lower Co and higher Ni contents (Fig. 8a). In this lithology, Co and Ni abundances vary inversely in kamacite (Fig. 8a). Metal outside the obvious shock-melt portion in lithology B has a low P content, similar to that of kamacite in the main lithology and in lithology A (Fig. 8b; note 5 in Table 2). However, the small kamacite grains in the shock-melted portion of this lithology have an elevated P content (up to
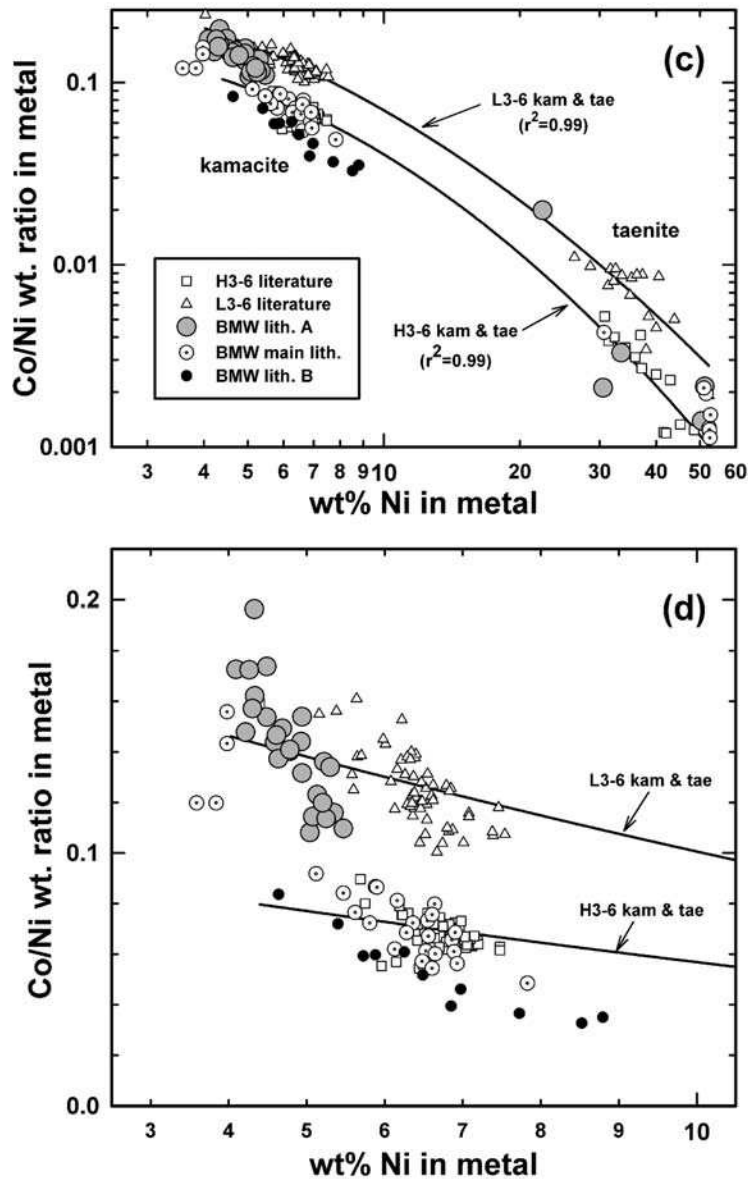
Fig. 8. *Continued.* Metal compositions in various lithologies of BMW compared to other H3–6 and L3–6 chondrites and to melting models. Metal compositions for typical H and L chondrites represent average compositions for individual meteorites (Afiattalab and Wasson 1980; Kong and Ebihara 1996; Kong et al. 1995; Rambaldi 1976, 1977; Rubin 1990; Smith et al. 1993), whereas BMW data represent individual analyses. c) Co/Ni versus Ni in metal from BMW and in H- and L-group chondrites. Regression lines are shown for H3–6 and L3–6 literature data. d) Enlargement of the low-Ni portion of part (c), showing distinct kamacite compositions in the three lithologies of BMW.

0.45 wt%) (Fig. 8b; note 6 in Table 2). In general, there is a positive correlation between P and Ni abundance in the kamacite grains from the shock-melted portion (Fig. 8b).

Figures 8c and 8d plot Co/Ni values against Ni contents in metal. This type of diagram is useful because H- and L-group metal Ni-Co trends are offset from one another (Rubin 1990; Brearley and Jones 1998), and because one expects subsolidus diffusional exchange between kamacite and taenite or tetrataenite to result in compositions moving along mixing lines between kamacite (relatively high Co/Ni) and high-Ni metal (relatively low Co/Ni) (Ruzicka et al. 2005).

Figure 8c shows that H3–6 and L3–6 kamacite and taenite have offset and excellent regressions (with r^2 correlation coefficients of 0.99).

Metal in the main lithology plots where one would expect for H-group kamacite and taenite (Figs. 8c and 8d). In lithology A, high-Ni metal (taenite and tetrataenite) mainly follows the H-group trend (the analysis with ~22 wt% Ni probably represents a mixture), but kamacite falls far off the regression trend for H chondrites and crosses the L chondrite regression line at a high angle (Fig. 8d). Lithology B kamacite forms a trend that is roughly parallel to the H-group trend, but

which is offset to lower Co/Ni values (Figs. 8c and 8d). Considering average compositions, kamacite in the three lithologies (A, main, and B) form an overall trend of inversely varying Co/Ni versus Ni, with lithology A having the highest Co/Ni (mean and standard deviation: 0.142 ± 0.022 wt ratio) and lowest Ni values (4.78 ± 0.40 wt%), the main lithology having intermediate Co/Ni (0.079 ± 0.026) and Ni values (6.02 ± 1.05), and lithology B having the lowest Co/Ni (0.052 ± 0.016) and highest Ni values (6.66 ± 1.29).

DISCUSSION

Metamorphism and Brecciation

Buck Mountain Wash is an H3–5 genomict breccia. All of the material in BMW belongs to the H group, based on silicate and metal compositions for the main lithology and olivine compositions for lithologies A and B. It is also apparent that BMW incorporated material of varying petrographic types. Lithology A is an H3.4–3.5 chondritic clast, and appears to lack any material of a higher petrographic type. The metamorphic grade of lithology B is more difficult to ascertain, but appears to consist of high type 3 or low type 4 material. The main lithology consists of a large proportion of H5 material with an admixture of type 3 and type 4 fragments, but does not appear to contain much (if any) type 6 material.

The main lithology of BMW is itself an intimately mixed breccia of type 3 through 5 material, and could be considered to be a fragmental breccia. Fragmental breccias consist of rock and mineral debris derived from one or more lithologies and resemble regolith breccias except for lacking evidence of solar wind–implanted gases or solar flare tracks (Rubin et al. 1983). The mixed materials in the main lithology of BMW are in the form of individual chondrules, chondrule fragments, and individual grains. This is unlike the fragmental breccias of Rubin et al. (1983) that consist of melt-rock or exotic clasts. The situation in BMW is more analogous to the fragmental breccias of Scott et al. (1985), who described type 4–6 chondrites that contain a few grains with aberrant compositions. However, the main lithology in BMW appears to contain a much larger compositional variety and a higher proportion of anomalous material than reported by Scott et al. (1985).

As BMW contains clasts of different petrographic types that are in direct contact with one another, and shows no evidence for metamorphic exchange between such clasts, metamorphism must have pre-dated brecciation. This is true both for the rock as whole (i.e., the various lithologies were metamorphosed to differing extents prior to the brecciation that brought them into contact) as well as for the main lithology itself (i.e., fine-scale brecciation postdated metamorphism). Postmetamorphic brecciation in ordinary chondrites is not especially rare (Binns 1967; Rubin et al.

1983; Scott et al. 1985). For example, 4 (19%) of the 21 H4–6 chondrites examined by Scott et al. (1985) experienced postmetamorphic brecciation.

Shock Reheating and Cooling

Heating and cooling effects related to shock were distinctly non-uniform in BMW. The main lithology was reheated the least. With a predominant shock stage of S2, the post-shock temperature increase for the main lithology was only ~20–50 °C (Stöffler et al. 1991). Lithology A was heated more substantially, being shocked to stage S5, producing polycrystalline kamacite; melting of troilite to form lacy troilite, veins, and droplets; localized melting of kamacite to form droplets; and probable melting of metal to form fizzy kamacite. Partial melting of metal and troilite in lithology A caused extensive shock blackening. Some silicate was also partially melted to produce melt pockets and glassy veins. Lithology A experienced a post-shock temperature increase of at least 300–600 °C and up to 850 °C to produce polycrystalline kamacite (Bennett and McSween 1996), and probably to ~950 °C or higher for a short period of time to produce localized eutectic melting of metal and troilite (e.g., Ruzicka et al. 2005). Lithology B was the most heated, as a portion of it experienced whole-rock melting (~1500–1750 °C) (Stöffler et al. 1991).

It has been suggested (e.g., Rubin 1995) that annealing following shock reheating could have been responsible for some thermal metamorphism in ordinary chondrites. The shock-blackened lithologies (A and B) in BMW suggest that the intensity of shock heating alone is not responsible for substantial metamorphism. Rather, it is the rate of post-shock cooling, or the presence of substantial amounts of shock melt, that can potentially cause thermal metamorphism.

The data for lithology A in BMW clearly show that an intense shock to S5 stage was incapable of resulting in significant thermal metamorphism. Lithology A is a type 3.4–3.5 chondrite that contains chondrule glass, inhomogeneous silicates, and sharply defined chondrules. After peak shock heating, temperature must have decreased rapidly.

Silicates in lithology B were more significantly heated. This lithology, which is now a high type 3 or a type 4 chondrite, could have been similar to the type 3 material in lithology A prior to shock. We suggest that the clast experienced more intense heating of silicate than lithology A because a portion of it contains a larger pocket of shock melt, which would have heated adjacent unmelted portions of the clast and transformed it into an equilibrated chondrite. The data for lithology B imply that larger-scale shock melting is potentially capable of resulting in significant thermal metamorphism of adjacent chondrite portions. A similar conclusion was reached by Rubin (1995) for Chico (L6) and Rose City (H5).

The high P content (>0.1 wt%) in the metal in the shock-melted portion of lithology B is notable. The remaining metal in lithology B is not rich in P, although all of the metal in lithology B is clearly related by low Co/Ni (Fig. 8). High P contents in metal were attributed by Smith and Goldstein (1977) to heating under reducing conditions, followed by rapid cooling. For an oxygen fugacity that is internally buffered by minerals in an H chondrite, one expects P to partition into metal at high temperatures, and into phosphate at low temperatures (e.g., Ruzicka et al. 2005). The high-P metal in BMW solidified from a whole-rock shock melt that allowed an approach to equilibrium at high temperatures. Phosphorus was evidently prevented from diffusing out of the metal grains because of rapid cooling. In contrast, other lithology B metal is low in P because it was not as extensively heated, and did not approach equilibrium at high temperatures.

Another notable feature of BMW is that it lacks martensite or plessite despite having experienced strong shock. Smith and Goldstein (1977) found martensite or decomposed martensite (plessite) in every strongly shocked chondrite they examined. The presence of this type of metal was attributed by these authors to reheating of metal to temperatures above 800 °C, followed by relatively rapid cooling (at rates more rapid than the extremely slow rates experienced by most iron meteorites). Clearly, lithologies A and B in BMW were heated to sufficiently high temperatures to potentially produce martensite or plessite, so their absence in BMW implies that subsolidus cooling was unusually slow for a strongly shocked chondrite.

Chemical Fractionation of Metal

A striking feature of BMW is the largely non-overlapping compositions of kamacite grains in the three lithologies (Fig. 8). Kamacite in the main lithology chemically resembles that in H chondrites, except for four texturally different grains that have lower Ni contents, two of which are also rich in Co (Figs. 8a and 8d). Kamacite in lithology A contains higher Co and lower Ni content, which resembles the kamacite in L chondrites except for having less Ni (Figs. 8a and 8d). Kamacite in lithology B has lower Co content, slightly higher Ni content on average, and lower Co/Ni values than in the main lithology and in H chondrites (Figs. 8a, 8c, and 8d).

Despite the similar Co contents of lithology A and L-group kamacite, it is unlikely that the two formed in a similar way. Rubin (1990) explained the difference between L-group and H-group kamacite as being caused by differences in fO_2 and subsolidus closure temperature related to systematic intergroup differences in grain sizes. According to Rubin (1990), higher fO_2 will cause more Fe to oxidize, leaving more Co and Ni in kamacite, and smaller metal grain sizes in L chondrites result in a lower closure temperature that results

in less Ni in kamacite. Although it is true that metal grains are smaller and less abundant in lithology A than in the main lithology, there is no evidence that lower closure temperatures can explain the anomalous composition of kamacite in lithology A, as this should also produce taenite with anomalously high Ni contents or abundant tetrataenite, which is not seen. Moreover, there is no evidence that metal in lithology A formed under more oxidizing conditions than in the main lithology, as this should have produced taenite with high Co contents.

Locally high concentrations of Co (up to 13 wt%) in kamacite (which may not be kamacite; see Rubin 1990) in Krymka (LL 3.1) have been attributed to shock processes (Semenenko and Perron 2005). The latter authors suggested that sulfurization of metal produced excess troilite and increased the cobalt and nickel contents of the metal. Our data are inconsistent with this being the explanation for the composition of lithology A kamacite, as there is an inverse relationship between cobalt and nickel contents in lithology A kamacite (best seen in Fig. 8d), rather than the positive correlation one might expect for the model of Semenenko and Perron (2005). Moreover, there is no evidence of excess troilite in lithology A as predicted by their model. Indeed, the opposite is true.

Instead, we note that the unusual Co and Ni content of kamacite in lithology A and B bracket typical H-group kamacite compositions (Fig. 8), and suggest that metal in lithologies A and B could have been derived by partial melting of typical H-group metal. In order to explain the observed kamacite compositions, Ni and Co would have to behave differently during partial melting of metal, with one element being compatible and the other being incompatible. Based on the parameterization of Chabot and Jones (2003), this condition is satisfied only when $D_{Co}^{SM/LM} > 1$ and $D_{Ni}^{SM/LM} < 1$ (where SM = solid metal and LM = liquid metal) at low sulfur contents ($X_S < 0.12$, where X_S = atom fraction of S in metallic melt). This implies a metallic melt deficient in S compared to an H chondrite metallic melt ($X_S = 0.14$ for fully molten metal-sulfide, and $X_S = 0.44$ for eutectic melt [Ruzicka et al. 2005]). If S can be removed, either in a vapor or melt phase, one could in principle make lithology A metal (high Co, low Ni) as a metallic residue of partial melting, and lithology B metal (low Co, high Ni) as a complementary metallic melt. A depletion in S is consistent with an apparently subchondritic amount of troilite in both lithologies A and B.

Trial calculations were made for equilibrium batch partial melting to see if kamacite with standard H-group composition could be converted into lithology A and B kamacite. The results show that the sense of the offsets can be explained, but that the magnitude of the differences cannot, because the partition coefficients are not far removed from a value of one. Thus, equilibrium partial melting cannot explain the compositions of kamacite grains in lithologies A and B.

In contrast, a fractional melting model comes closer to explaining the composition of lithology A metal. Perfect fractional melting involves the removal of liquid from solid as soon as it forms, with only the last solid considered to be in equilibrium with the final melt that is produced. Figure 8a shows the compositions of metallic solids and liquids produced by fractional melting for X_S = 0.05 and 0.07, which intersect at the assumed starting composition equal to average H-group kamacite. The composition of solids and liquids for a given sulfur content track each other closely, but for any given melting degree, the solids have higher Co and lower Ni contents than the liquids. The composition of residual solid is equal to that of the starting metal at the onset of melting, and becomes similar to lithology A kamacite with 85–99% melting (Fig. 8a). Although some of the less extreme compositions in lithology A kamacite can also be attained in liquids produced by 90–99% fractional melting, the most Co-rich and Ni-poor grains cannot be explained as liquids.

These model results for lithology A imply that for perfect fractional crystallization, ~85–99% melting is required, that much of the lithology A metal is composed of a small amount of solid residue from which large amounts of liquid were removed, and that this melt was sulfur-bearing (X_S = 0.05–0.07). If metallic melt was removed from lithology A to leave behind a residue composition, this would explain the smaller sizes of metal grains in lithology A, and the dearth of metal in the border zones of this lithology (Figs. 1a and 1c).

However, *perfect* fractional crystallization cannot be the mechanism that created lithology A metal. It is clear that while lithology A has less metal than is typical for an H chondrite, it has not lost 80–99% of its original metal. Additionally, this process should have removed all sulfur in the metallic melt at an early stage when the degree of melting was small. The model results imply 5–7 at% S in the final melt, but all sulfur should have been removed in the *first* melt at the eutectic temperature. Thus, if the D-value parameterization of Chabot and Jones (2003) is applicable, not all of the early melt could have been removed from the solid, and the process involved in making lithology A metal could not have been one of strict fractional melting. Instead, some early formed and presumably S-rich liquid must have been kept in contact with solid metal throughout the melting process. Alternatively, the D-value parameterization of Chabot and Jones (2003) may not be valid for this case. This could arise if disequilibrium were important. Disequilibrium would not be surprising if the melting process was very fast, as would be expected for a shock-generated partial melt.

Model results show that neither equilibrium nor fractional melting can explain the compositions of kamacite in lithology B. Some disequilibrium must have been involved in forming this metal, as the variable and high P contents imply incomplete equilibration (see the Shock Reheating and Cooling section). We suggest that this metal could have formed in part by reduction of FeO to Fe-metal during the shock-melting event that affected lithology B. This reduction process would dilute Co in the metal, lowering its Co content. To account for the slight enrichment in average Ni content of lithology B metal compared to that in the main lithology, either some NiO could have been reduced to Ni metal, or some Ni-rich melt could have been incorporated into lithology B metal.

Assembly of Buck Mountain Wash

Textures and phase chemistries suggest that multiple shock events were responsible for assembling and compacting individual components of BMW and for the lithification of the meteorite. We can identify various shock processes that occur earlier or later during the formation of BMW. Among the earlier events is the formation of the separate components of BMW, including lithologies A and B and the main lithology.

Lithology A appears to have formed in a region on the H-group parent body that consisted entirely of type 3 material. There is no evidence for any material of a higher petrographic type in this clast, which has been heavily deformed (see the Lithology A section of this paper). The deformation created a foliated texture, with metal grains and elongated chondrules pressed tightly together, leaving little room for rare isolated patches of intervening matrix (Figs. 4a and 4b). To become foliated, either chondrules rotated in place or experienced plastic deformation. It is possible that both processes occurred. Brecciated chondrule margins (Figs. 4a and 4b) imply mechanical movement (rotation), whereas intense plastic deformation of olivine (consistent with shock stage S5) suggests the possibility of ductile deformation of chondrules. The direction of foliation is consistent across the portion of lithology A studied in two adjacent thin sections, and does not correspond to the boundary between lithology A and the main lithology, suggesting that this foliation formed in a shock event preceding incorporation into BMW. This same early shock event may also have included fractional or disequilibrium melting to produce the unusual kamacite compositions in lithology A (see the Metal section and the Chemical Fractionation of Metal section).

Lithology B also formed early, in a portion of the parent body possibly proximal to where lithology A originated. The chemical data for silicates in lithology B suggest that it is a high type 3 or low type 4 chondrite (see the Silicates section), possibly similar to lithology A originally (see the Shock Reheating and Cooling section). As with lithology A, it lacks the fragmental texture of the main lithology, suggesting that it originated in a region on the H-group parent body consisting of one petrographic type. Also like lithology A, lithology B was heavily deformed and shock-blackened. However, unlike lithology A, there is no evidence for foliation of silicates or metal in lithology B. Instead, one portion of this clast experienced whole-rock impact melting. The shock-

blackening of lithology B truncates abruptly at the contact with the main lithology, suggesting that it resulted from a shock event prior to incorporation into BMW. The whole-rock melt in lithology B experienced rapid cooling at high temperatures (see the Shock Reheating and Cooling section). The kamacite in the entire clast, including the melted and unmelted portions, also experienced chemical fractionation, probably by reduction during this early shock event (see the Chemical Fractionation of Metal section).

In thin section, the main lithology is reminiscent of a type 5 chondrite (see the Main Lithology section). However, unlike a typical chondrite containing chondrules separated by recrystallized matrix, the main lithology of BMW consists primarily of fragments ranging widely in size. The material between larger chondrule fragments is not recrystallized matrix, but rather a collection of smaller fragments and individual grains (Fig. 2d). The contacts between the three lithologies are sharp, suggesting that prior to the incorporation of lithologies A and B, the main lithology must have experienced intense brecciation which mixed materials of different petrologic types on an intimate scale. Most of this material was type 5, but some type 3 and type 4 material was also intermixed. Although it is conceivable that the type 3 material found within the main lithology was introduced at the same time as the incorporation of lithologies A and B, this is unlikely, as the type 3 material in the main lithology is not intensely shocked. The polymict and fragmental character of the main lithology suggests that it originated in a regolith that experienced multiple impacts.

A relatively late event was the assembly of the three lithologies into BMW. This probably involved an impact that compacted and lithified the rock, but did not involve a strong shock (≤S2–S3). The incorporation of lithology A into BMW resulted in some foliation in the main lithology, producing the preferential alignment of metal and silicates near the contact with A (see the Main Lithology section). The foliation is consistent with the mobilization of metal in a stress field. The metal embayment textures in the main lithology strongly suggest that metal was fluidized and injected between and within chondrules. Some of the apparent fluidization of metal in the main lithology may have occurred at this time, as such metal grains are part of the foliation. The metal-depleted boundary of lithology A, which borders the main lithology, must also have been formed upon assembly when the two lithologies came into contact with one another. Metal lost from the border zone of A does not appear to have moved into the adjacent main lithology, as there is no excess of metal in the main lithology (Fig. 1c). It is possible that some of the fine opaque veins and droplets throughout lithology A formed at this time. In any case, metal was mobilized in both the main lithology and in lithology A during the final assembly of BMW.

We suggest that such mobilization, together with the foliation produced in the main lithology, could indicate that lithology A and the main lithology were somewhat warm and ductile when they were brought into contact with one another. However, the breccia contact between lithology A and main lithology is sharp and shows no evidence for chemical exchange, suggesting that the materials were not warm for very long. In contrast, lithology B appears to have been fairly cold when it was brought into contact with the main lithology, as it shows no evidence for metal mobilization in the unmelted portion. As further support for the assembly of lithology B while it was cold, we note that the B–main contact is sharp and shows no evidence for chemical exchange.

Although multiple weak impact events are required to form the main lithology of BMW, it is possible that the intense shock which affected lithologies A and B may have occurred at the same time, as different manifestations of the same event. It is also possible that the shock event(s) that affected these lithologies was an early stage of the same shock event that eventually assembled and lithified BMW. The rapid cooling experienced by all lithologies at high temperature and the slower cooling experienced at lower temperature (see the Shock Reheating and Cooling section) implies that BMW was lithified in a deep regolith setting, at sufficient depth to prevent rapid cooling at low temperatures, but still sufficiently close to the surface of the parent body where impact events could have strongly affected the components.

CONCLUSIONS

The Buck Mountain Wash chondrite is a new H-group genomict breccia from the Franconia strewn field that experienced complex shock processes, including small-scale brecciation, mobilization and melting of metal and troilite, chemical fractionation of metal, localized silicate melting, and shock-induced foliation and compaction. Three lithologies with varied metamorphic and shock histories were identified. The main lithology is a weakly shocked (predominantly shock stage S2) fragmental microbreccia (fragmented on such a small scale that fragments are comparable to the scale of individual chondrules). It consists primarily of heavily metamorphosed (type 5) material in which weakly metamorphosed (type 3 and 4) material was finely intermixed. This lithology possibly formed by repeated impacts in the regolith of the parent body. A second lithology (A) is a type 3 chondrite clast that was intensely shocked (up to shock stage S5), but which was not significantly shock-annealed, owing to rapid cooling at high temperatures. The third lithology (B) is a weakly metamorphosed (high type 3/ low type 4) clast that was locally shock-melted. Two different mechanisms were involved in impact-induced chemical fractionation of metal. Kamacite in lithology A appears to have formed largely as a residue during imperfect fractional or disequilibrium partial melting, whereas kamacite in lithology B appears to have formed by melting accompanied by FeO-reduction. The components of BMW cooled more

slowly at low temperatures than other heavily shocked chondrites, suggesting that BMW was shock-compacted and lithified at moderate depth in the regolith of its parent body.

Editorial Handling—Dr. Edward Scott

REFERENCES

Afiattalab F. and Wasson J. T. 1980. Composition of the metal phases in ordinary chondrites: Implications regarding classification and metamorphism. *Geochimica et Cosmochimica Acta* 44:431–446.

Bennett M. E. III and McSween H. Y., Jr. 1996. Shock features in iron-nickel metal and troilite of L-group ordinary chondrites. *Meteoritics & Planetary Science* 31:255–264.

Binns R. A. 1967. Structure and evolution of non-carbonaceous chondritic meteorites. *Earth and Planetary Science Letters* 2:23–28.

Bleacher L. V., Huss G. R., Leshin L. A., Miller M., Garcia R., Clary S., Gwilliam J., and Sloan L. 2005. Meteorites from the Franconia, Arizona area: Observations and summary of petrographic characteristics (abstract #1807). 36th Lunar and Planetary Science Conference. CD-ROM.

Brearley A. J. and Jones R. H. 1998. Chondritic meteorites. In *Planetary materials,* edited by J. J. Papike. Washington, D.C.: Mineralogical Society of America. pp. 3-1–3-398.

Chabot N. L. and Jones J. H. 2003. The parameterization of solid metal-liquid metal partitioning of siderophile elements. *Meteoritics & Planetary Science* 38:1425–1436.

Dodd R. T. 1981. *Meteorites: A petrologic-chemical sysnthesis.* Cambridge: Cambridge University Press. 368 p.

Hutchison R. 2004. *Meteorites: A petrologic, chemical and isotopic synthesis.* Cambridge: Cambridge University Press. 506 p.

Kong P. and Ebihara M. 1996. Metal phases of L chondrites: Their formation and evolution in the nebula and in the parent body. *Geochimica et Cosmochimica Acta* 60:2667–2680.

Kong P., Ebihara M., Nakahara H., and Endo K. 1995. Chemical characteristics of metal phases of the Richardton H5 chondrite. *Earth and Planetary Science Letters* 136:407–419.

Rambaldi E. R. 1976. Trace element content of metals from L-group chondrites. *Earth and Planetary Science Letters* 31:224–238.

Rambaldi E. R. 1977. Trace element content of metals from H- and LL-group chondrites. *Earth and Planetary Science Letters* 36:347–358.

Rubin A. E. 1990. Kamacite and olivine in ordinary chondrites: Intergroup and intragroup relationships. *Geochimica et Cosmochimica Acta* 54:1217–1232.

Rubin A. E. 1992. A shock-metamorphic model for silicate darkening and compositionally variable plagioclase in CK and ordinary chondrites. *Geochimica et Cosmochimica Acta* 56:1705–1714.

Rubin A. E. 1995. Petrologic evidence for collisional heating of chondritic asteroids. *Icarus* 113:156–167.

Rubin A. E., Rehfeldt A., Peterson E., and Keil K. 1983. Fragmental breccias and the collisional evolution of ordinary chondrite parent bodies. *Meteoritics* 18:179–196.

Russell S. S., Folco L., Grady M. M., Zolensky M. E., Jones R., Righter K., Zipfel J., and Grossman J. N. 2004. The Meteoritical Bulletin, No. 88. *Meteoritics & Planetary Science* 39:A215–A272.

Russell S. S., Zolensky Y. M., Righter K., Folco L., Jones R., Connolly H. C., Jr., Grady M. M., and Grossman J. N. 2005. The Meteoritical Bulletin, No. 89. *Meteoritics & Planetary Science* 40:A201–A263.

Ruzicka A., Killgore M., Mittlefehldt D. W., and Fries M. 2005. Portales Valley: Petrology of a metallic-melt meteorite breccia. *Meteoritics & Planetary Science* 40:261–296.

Scott E. R. D. 1984. Classification, metamorphism, and brecciation of type 3 chondrites from Antarctica. *Smithsonian Contributions to the Earth Sciences* 26:73–94.

Scott E. R. D. and Krot A. N. 2005. Chondrites and their components. In *Meteorites, comets, and planets.* Treatise on Geochemistry, vol. 1, edited by Davis A. M. Amsterdam: Elsevier. pp. 143–200.

Scott E. R. D., Lusby D., and Keil K. 1985. Ubiquitous brecciation after metamorphism in equilibrated ordinary chondrites. Proceedings, 16th Lunar and Planetary Science Conference. pp. D137–D148.

Sears D. W. G. and Dodd R. T. 1988. Overview and classification of meteorites. In *Meteorites and the early solar system,* edited by Kerridge J. F. and Matthews M. S. Tucson, Arizona: The University of Arizona Press. pp. 3–31.

Semenenko V. P. and Perron C. 2005. Shock-melted material in the Krymka LL3.1 chondrite: Behavior of the opaque minerals. *Meteoritics & Planetary Science* 40:173–185.

Smith B. A. and Goldstein J. I. 1977. The metallic microstructures and thermal histories of severely reheated chondrites. *Geochimica et Cosmochimica Acta* 41:1061–1072.

Smith D. G. W., Miura Y., and Launspach S. 1993. Fe, Ni and Co variations in the metals of some Antarctic chondrites. *Earth and Planetary Science Letters* 120:487–498.

Stöffler D., Keil K., and Scott E. R. D. 1991. Shock metamorphism of ordinary chondrites. *Geochimica et Cosmochimica Acta* 55:3845–3867.

Wlotzka F. 1993. A weathering scale for the ordinary chondrites (abstract). *Meteoritics* 28:460.